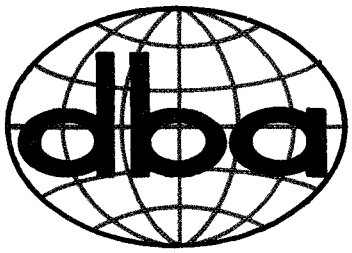

DBA SYSTEMS, INC.

IN-FLIGHT CALIBRATION
OF THE
APOLLO 14 500MM HASSELBLAD CAMERA

Photogrammetry

Computer Services

Mathematical Research

Electro-Optical Instrumentation

GENERAL OFFICES
Post Office Drawer 550
Melbourne, Florida 32901
Phone: 305 727-0660

ELECTRO-OPTICAL DIV.
Post Office Drawer 550
Melbourne, Florida 32901
Phone: 305 727-2020

WASH. D.C. OFFICE
9301 Annapolis Road
Lanham, Maryland 20801
Phone: 301 577-3001

CR-115176

IN-FLIGHT CALIBRATION OF THE APOLLO 14 500MM HASSELBLAD CAMERA

Final Report

Prepared for:

National Aeronautics and Space Administration

Manned Spacecraft Center
Mapping Sciences Laboratory
Houston, Texas

Contract: NAS9-11667

Prepared by:

John F. Kenefick
Maurice S. Gyer
Bill F. Harp
DBA Systems, Inc.
P.O. Drawer 550
Melbourne, Florida

1 September 1971

ABSTRACT

A modified reconnaissance camera flown on the APOLLO 14 mission was to have provided photographs for mapping the tentative APOLLO 16 landing site near Descartes, but a malfunction of the camera necessitated compilation with backup photographs secured with a 500mm Hasselblad camera. The Hasselblad had not been rigorously calibrated prior to the mission and quarantine regulations prevented an immediate post-flight calibration. Convergent photographs which had been secured while in lunar orbit provided excellent material for performing an in-flight calibration. Three frames from each of three passes over Desartes were measured and processed through a recently developed "self-calibration" program in which the elements of interior orientation and lens distortion are treated as variable parameters and are recovered analytically, without the necessity of absolute control in object space. A brief mathematical outline for analytical self-calibration is presented with the results of the Hasselblad calibration. In addition, the results of several simulations are presented to demonstrate the precision with which cameras may be self-calibrated on future lunar missions given specific, but reasonable, photographic geometry.

TABLE OF CONTENTS

LIST OF TABLES

LIST OF ILLUSTRATIONS

1.0 INTRODUCTION

APOLLO 14 was the first lunar mission to successfully secure metric photographs of the lunar surface. The primary function of the Lunar Topographic Camera (described briefly by Doyle (1970)), was to secure photographs for mapping future APOLLO landing zones. Before photographs were secured of the APOLLO 16 site near Descartes, however, the camera failed, leaving only backup photographs obtained with a 500 mm Hasselblad for compilation of the charts.

Because the Hasselblad photographs were not expected to be used for mapping, a rigorous preflight calibration of the camera had not been obtained. Moreover, an immediate post-flight calibration was hampered by normal quarantine restrictions. Faced with pressing compilation schedules, NASA contracted DBA to perform a calibration using the actual photographs which had been secured with the camera while in lunar orbit. Fortunately, the photographs had been deliberately exposed in a convergent fashion to increase the precision of "heighting" during compilation. This very convergence was of pivotal importance for extracting a calibration of the camera as well.

The method employed for the Hasselblad calibration is based upon the principles of self-calibration developed in Brown (1958) and Brown, Bush and Sibol (1963 and 1964). Originally, the analytical self-calibration program was developed for in-house use in conjunction with precision close range photogrammetric projects (Kenefick (1971)). Recent extensive experiments with the technique demonstrated that certain configurations of convergent photographs would lead to a complete calibration of the inner cone without any external information whatsoever. In the following sections, a brief mathematical outline for analytical self-calibration is presented with the results of the Hasselblad calibration. In addition, the results of simulated lunar photographic sequences are presented to demonstrate the potential for in-flight analytical self-calibration on future APOLLO missions.

2.0 ANALYTICAL SELF-CALIBRATION

The mathematical basis for analytical self-calibration is derived from the earlier work of Brown, Davis and Johnson (1964) and Brown (1968). In Brown, Davis and Johnson a completely general formulation was developed wherein very large photogrammetric blocks could be reduced in a simultaneous manner, solving for the elements of exterior orientation of all photographs as well as the ground coordinates of the passpoints. In addition, a technique was presented which allowed introduction of a priori constraints on any of the exterior projective parameters and/or ground points by treating a priori knowledge as direct observations of the parameters. However, a model describing all parameters of the inner cone $(x_p, y_p, c, k_1, k_2, k_3, p_1, p_2)$ as variables subject to adjustment was not included, although a completely general formulation was given which would admit these parameters.

In Brown (1968) the Aerial SMAC[1] technique for in-flight calibration was developed which, in contrast to the work of Brown, Davis and Johnson was designed to recover the parameters of the inner cone rather than ground coordinates of the passpoints. In fact, Aerial SMAC was predicated on the assumption that the photographs would be secured over a very precise targeted test range and, therefore, no provision was made for the recovery or adjustment of ground coordinates. Subsequent experience with Aerial SMAC, however, showed that the assumption of an "errorless" ground survey could oftentimes be a practical limitation of an otherwise powerful method of calibration. As a result of our experiences with Aerial SMAC a modified program, which we refer to as our self-calibration scheme, has been developed in-house. In essence, the program is a simultaneous block analytical aerotriangulation program which carries the elements of the inner cone as parameters to be recovered in the adjustment along with the elements of exterior orientation and the ground coordinates of the passpoints.

---

[1] SMAC is the DBA acronym for Simultaneous Multiframe Analytical Calibration.

Originally, the self-calibration program was adapted to the calibration of cameras used in precision close range photogrammetry where the construction and maintenance of a coordinated test range, of sufficient relative accuracy so as not to contaminate the calibration, was a practical impossibility. Recent experiments with the program in conjunction with highly convergent close range photographs demonstrated that very sharp calibrations could indeed be determined[1], without any absolute control in object space. The technique was also successfully applied to the calibration of two Hasselblad cameras which had been used to photograph explosive bolts on the launch vehicle of the original Orbiting Astronomical Observatory which failed to achieve orbit. (A subsequent investigation into the cause of the failure required photogrammetric reductions of these photographs; Brown, Kenefick, and Harp (1971)). With this experience in hand, then, the application of the technique to calibrating the 500mm Hasselblad camera was a natural course of action.

2.1 Fundamental Observational Equations

The projective or collinearity equations of analytical photogrammetry provide the basic framework for the analytical calibration scheme. Inasmuch as the parameters of the inner cone are to be recovered simultaneously in a block triangulation, the projective equations are augmented with the parameters of the inner cone:

[1] Certain configurations of convergent photographs do not lead to a full calibration of the inner cone. A discussion of geometric considerations is given in Section 2.3.

$$x_{ij} - x_p + \bar{x}_{ij}(k_1 r_{ij}^2 + k_2 r_{ij}^4 + k_3 r_{ij}^6) + p_1(r_{ij}^2 + 2\bar{x}_{ij}^2) + 2p_2\,\bar{x}_{ij}\,\bar{y}_{ij}$$

$$= c \cdot \frac{(X_j - X_i^c)A_i + (Y_j - Y_i^c)B_i + (Z_j - Z_i^c)C_i}{(X_j - X_i^c)D_i + (Y_j - Y_i^c)E_i + (Z_j - Z_i^c)F_i} \qquad (1)$$

$$y_{ij} - y_p + \bar{y}_{ij}(k_1 r_{ij}^2 + k_2 r_{ij}^4 + k_3 r_{ij}^6) + 2p_1\,\bar{x}_{ij}\,\bar{y}_{ij} + p_2(r_{ij}^2 + 2\bar{y}_{ij}^2)$$

$$= c \cdot \frac{(X_j - X_i^c)A_i' + (Y_j - Y_i^c)B_i' + (Z_j - Z_i^c)C_i'}{(X_j - X_i^c)D_i + (Y_j - Y_i^c)E_i + (Z_j - Z_i^c)F_i}$$

in which,

x_{ij}, y_{ij} = photographic coordinates of the j th ground point on the i th photograph, referred to the indicated principal point as origin

x_p, y_p = photographic coordinates of the principal point of photogrammetry; assumed constant over all photographs

$\bar{x}_{ij} = x_{ij} - x_p$

$\bar{y}_{ij} = y_{ij} - y_p$

$r_{ij} = (\bar{x}_{ij}^2 + \bar{y}_{ij}^2)^{\frac{1}{2}}$

k_1, k_2, k_3 = correction coefficients for Gaussian symmetric radial distortion; assumed constant over all photographs

p_1, p_2 = correction coefficients for decentering distortion; assumed constant over all photographs

c = Gaussian focal length; assumed constant over all photographs

$\left.\begin{matrix} A, B, C \\ A', B', C' \\ D, E, F \end{matrix}\right\}_i$ = Elements of the orthogonal orientation matrix T of the i th photograph; functions of three rotation angles $\varphi_i, \omega_i, \kappa_i$

$$T_i = \begin{bmatrix} A & B & C \\ A' & B' & C' \\ D & E & F \end{bmatrix}_i = \begin{bmatrix} c\varphi c\kappa & c\omega s\kappa - s\omega s\varphi c\kappa & s\omega s\kappa + c\omega s\varphi c\kappa \\ -c\varphi s\kappa & c\omega c\kappa + s\omega s\varphi s\kappa & s\omega s\kappa - c\omega s\varphi s\kappa \\ -s\varphi & -s\omega c\varphi & c\omega c\varphi \end{bmatrix}_i$$

X_i^c, Y_i^c, Z_i^c = object space coordinates of the i th exposure station

X_j, Y_j, Z_j = object space coordinates of the j th ground point.

Starting with the measured quantities x_{ij}, y_{ij}, and an initial approximation for each unknown parameter, equations (1) are linearized by Taylor's series expansion. When all linearized equations are gathered we may represent this collection of equations in matrix notation as:

$$v + \dot{B}\dot{\delta} + \ddot{B}\ddot{\delta} + \dddot{B}\dddot{\delta} = \epsilon \qquad (2)$$

where,

$v_{(2mn,1)}$ = vector of photographic measurement residuals

$\dot{B}_{(2mn,s)}$ = matrix of partial derivatives of equations (1) with respect to the parameters of the inner cone; evaluated with measured quantities and current values of the unknown parameters

$\dot{\delta}_{(s,1)}$ = vector of corrections to be applied to current values of the parameters of the inner cone

$\ddot{B}_{(2mn,6m)}$ = matrix of partial derivatives of equations (1) with respect to the elements of exterior orientation; evaluated with measured quantities and current values of the unknown parameters

$\ddot{\delta}_{(6m,1)}$ = vector of corrections to be applied to current values of the elements of exterior orientation

$\dddot{B}_{(2mn,3n)}$ = matrix of partial derivatives of equations (1) with respect to the coordinates of the ground points; evaluated with measured quantities and current values of the unknown parameters

$\dddot{\delta}_{(3n,1)}$ = vector of corrections to be applied to current values of the coordinates of the ground points

$\epsilon_{(2mn,1)}$ = discrepancy vector resulting from evaluation of equations (1) with measured quantities and current values of the unknown parameters

m = total number of photographs

n = total number of ground points.

In addition to the basic observational equations (2), we also have supplemental observation equations arising from a priori knowledge regarding any of the parameters carried in equations (1). For convenience the supplemental equations are grouped according to the subset of parameters involved:

$$\dot{v} - \dot{\delta} = \dot{\epsilon} \qquad \text{(inner cone)} \tag{3}$$

$$\ddot{v} - \ddot{\delta} = \ddot{\epsilon} \qquad \text{(exterior orientations)} \tag{4}$$

$$\dddot{v} - \dddot{\delta} = \dddot{\epsilon} \qquad \text{(ground points)} \tag{5}$$

where,

$\underset{(s,1)}{\dot{v}}$ = vector of observation residuals for the parameters of the inner cone

$\underset{(s,1)}{\dot{\delta}}$ = vector of corrections to be applied to current values of the parameters of the inner cone

$\underset{(s,1)}{\dot{\epsilon}}$ = discrepancy vector; differences between a priori values and current values of the parameters of the inner cone

$\underset{(s_m,1)}{\ddot{v}}$ = vector of observation residuals for the elements of exterior orientation

$\underset{(s_m,1)}{\ddot{\delta}}$ = vector of corrections to be applied to current values of the elements of exterior orientation

$\underset{(s_m,1)}{\ddot{\epsilon}}$ = discrepancy vector; differences between a priori values and current values of the elements of exterior orientation

$\underset{(3n,1)}{\dddot{v}}$ = vector of observation residuals for the coordinates of the ground points

$\underset{(3n,1)}{\dddot{\delta}}$ = vector of corrections to be applied to current values of the coordinates of the ground points

$\underset{(3n,1)}{\dddot{\epsilon}}$ = discrepancy vector; differences between a priori values and current values of the coordinates of the ground points

The entire set of observation equations (2), (3), (4), and (5) may be merged into a single expression which is conveniently written as:

$$\bar{v} + \bar{B}\bar{\delta} = \bar{\epsilon} \tag{6}$$

in which,

$$\underset{(k,1)}{\bar{v}} = (v, \dot{v}, \ddot{v}, \dddot{v})^T; \quad \underset{(k,\ell)}{\bar{B}} = \begin{bmatrix} \dot{B} & \ddot{B} & \dddot{B} \\ -I & 0 & 0 \\ 0 & -I & 0 \\ 0 & 0 & -I \end{bmatrix}$$

$$\underset{(\ell,1)}{\bar{\delta}} = (\dot{\delta}, \ddot{\delta}, \dddot{\delta})^T; \quad \underset{(k,1)}{\bar{\epsilon}} = (\epsilon, \dot{\epsilon}, \ddot{\epsilon}, \dddot{\epsilon})^T$$

$$k = 2mn + 8 + 6m + 3n; \quad \ell = 8 + 6m + 3n.$$

The covariance matrix associated with the merged observation equations is:

$$\underset{(k,k)}{\bar{\Lambda}} = \begin{bmatrix} \Lambda & & & \\ & \dot{\Lambda} & & \\ & & \ddot{\Lambda} & \\ & & & \dddot{\Lambda} \end{bmatrix}$$

where,

$\underset{(2mn,2mn)}{\Lambda}$ = covariance matrix for the measured photographic coordinates; 2x2 block diagonal when independence of image coordinates is assumed

$\underset{(8,8)}{\dot{\Lambda}}$ = covariance matrix for the parameters of the inner cone

$\underset{(6m,6m)}{\ddot{\Lambda}}$ = covariance matrix for the elements of exterior orientation; 6x6 block diagonal

$\underset{(3n,3n)}{\dddot{\Lambda}}$ = covariance matrix for the coordinates of the ground points; 3x3 block diagonal when independence of ground points is assumed.

2.2 The General Normal Equations and Solution

By definition, a least squares adjustment must provide the vectors $\bar{v}$ and $\bar{\delta}$ which satisfy equation (6) and at the same time minimizes the quadratic $\bar{v}^T \bar{\Lambda}^{-1} \bar{v}$. The so called normal equations leading to this solution has been shown by Brown (1955) to be:

$$(\bar{B}^T \bar{\Lambda}^{-1} \bar{B})\bar{\delta} = \bar{B}^T \bar{\Lambda}^{-1} \bar{\epsilon} . \tag{7}$$

After performing indicated operations and substituting previous notations we have the general form of the normal equations:

$$\begin{bmatrix} \dot{N}+\dot{W} & \bar{N} & \bar{\bar{N}} \\ \bar{N}^T & \ddot{N}+\ddot{W} & \bar{\bar{N}} \\ \bar{\bar{N}}^T & \bar{\bar{N}}^T & \dddot{N}+\dddot{W} \end{bmatrix} \cdot \begin{bmatrix} \dot{\delta} \\ \ddot{\delta} \\ \dddot{\delta} \end{bmatrix} = \begin{bmatrix} \dot{c} - \dot{W}\dot{\epsilon} \\ \ddot{c} - \ddot{W}\ddot{\epsilon} \\ \dddot{c} - \dddot{W}\dddot{\epsilon} \end{bmatrix} \tag{8}$$

in which,

$$\underset{(8,8)}{\dot{N}} = \dot{B}^T W \dot{B}; \quad \underset{(8,1)}{\dot{c}} = \dot{B}^T W \epsilon$$

$$\underset{(8,6m)}{\bar{N}} = \dot{B}^T W \ddot{B}; \quad \underset{(8,3n)}{\bar{\bar{N}}} = \dot{B}^T W \dddot{B}$$

$$\underset{(6m,6m)}{\ddot{N}} = \ddot{B}^T W \ddot{B}; \quad \underset{(6m,1)}{\ddot{c}} = \ddot{B}^T W \epsilon$$

$$\underset{(6m,3n)}{\bar{\bar{N}}} = \ddot{B}^T W \dddot{B}$$

$$\underset{(3n,3n)}{\dddot{N}} = \dddot{B}^T W \dddot{B}; \quad \underset{(3n,1)}{\dddot{c}} = \dddot{B}^T W \epsilon$$

$$W = \Lambda^{-1}; \quad \dot{W} = \dot{\Lambda}^{-1}; \quad \ddot{W} = \ddot{\Lambda}^{-1}; \quad \dddot{W} = \dddot{\Lambda}^{-1}.$$

Equation (8) is solved with a first order partitioning scheme by elimination of the ground points so as to form the "reduced" normal equations as described in Brown, Davis, and Johnson (op. cit.). The practicality of solving such a reduced system is obvious when consideration is given to the sizes of the matrices requiring inversion. The matrices to be inverted are of rank and order $(8+6m) \times (8+6m)$ and $(3n) \times (3n)$, the latter corresponding to the $(\dddot{N} + \dddot{W})$ matrix. Now the inversion of $(\dddot{N} + \dddot{W})$ is extremely simple inasmuch as the computational effort requires nothing more than inverting a series of 3×3 sub-matrices. It would appear then, that the bulk of the effort would be associated with inversion of an $(8+6m) \times (8+6m)$ matrix. However, when convergent photographs are used, a typical reduction requires fewer than a dozen frames to recover a precise calibration. Thus, in practice, the actual rank of the $(8+6m) \times (8+6m)$ matrix does not become too great to be readily inverted by a standard Gaussian elimination. Of course, the square roots of the first eight elements of the inverse of this matrix provide posteriori standard deviations for the adjusted parameters of the inner cone.

2.3 The Requirement For Convergent Photographs

As mentioned earlier, the process of pure self-calibration requires that the photographs be highly convergent when absolute constraints in object space or at the exposure stations are not available. Although provision was made in the foregoing mathematical development for admitting external constraints, it is the very desirability of eliminating the need for such a priori knowledge that has led to the implementation of convergent photographs. Advantages of convergent photographs relative to near vertical photographs become quite apparent when certain partial derivatives of the projective equations are examined. For instance:

$$\frac{\partial x_p}{\partial X_i^c} = \frac{-x_{ij} D_i - c A_i}{(X_j - X_i^c)D_i + (Y_j - Y_i^c)E_i + (Z_j - Z_i^c)F_i} \cdot \tag{9}$$

As equation (9) stands there is no general projective relationship between x_p and X_i^c. However, when near vertical photographs are introduced (i.e. $\varphi_i = \omega_i \approx 0$) the C, C', D, and E elements of the orientation matrices also approach zero and equation (9) degenerates to:

$$\frac{\partial x_p}{\partial X_i^c} \approx - \frac{c}{(Z_j - Z_i^c)} \cdot \cos \varkappa_i \cdot \tag{10}$$

As a general rule variations of relief in object space (Z_j) are small relative to Z_i^c and if $\varkappa_i = 0$ equation (10) is simplified further to:

$$\frac{\partial x_p}{\partial X_i^c} \approx \frac{c}{Z} \tag{11}$$

where,

Z = flying height above mean terrain.

Thus from equation (11) we see that an exact (within stated assumptions) projective relation exists between x_p and X_i^c when the photographs are near vertical, but when the photographs are convergent equation (9) may not be simplified and no projective compensation exists. Similar analyses may be developed for $\partial x_p/\partial Y_i^c$, $\partial y_p/X_i^c$, $\partial y_p/Y_i^c$, and $\partial c/\partial Z_i^c$.

Even though convergence of the photographs will uncouple projective compensations between interior orientation and X^c, Y^c, Z^c, convergence alone will not allow a complete recovery of the parameters of the inner cone. When the primary mechanisms of projective compensation are not allowed to act, either by convergence and/or external constraints, secondary compensations begin to act (especially with narrow angle cameras) and they too must be counteracted. As an example:

$$\frac{\partial x_p}{\partial \varphi_i} = \frac{c^2 + x_{ij}^2}{c} \cos \varkappa_i - \frac{x_{ij}\, y_{ij}}{c} \sin \varkappa_i \,. \tag{12}$$

Note that the right hand side of equation (12) is completely independent of φ and ω (i.e. convergence). Now if <u>all</u> photographs are exposed with $\varkappa_i \approx 0$, for example, equation (12) is reduced to:

$$\frac{\partial x_p}{\partial \varphi_i} = c + \frac{x_{ij}^2}{c} \,. \tag{13}$$

Obviously as c becomes large relative to x and y perfect compensation is again approached. Thus, to affect a complete recovery of the parameters of the inner cone without external attitude constraints, it becomes necessary to expose the photographs with differential $\varkappa$ angles as well as in a convergent mode.

3.0 RESULTS OF THE HASSELBLAD CALIBRATION

3.1 Description of the Photographs

On revolutions 27, 28, and 30 of the APOLLO 14 mission a special spacecraft maneuver over the tentative APOLLO 16 landing zone allowed convergent photographs to be secured with the high resolution 500mm Hasselblad camera. The purpose of the maneuver and convergent photographic mode was to improve the precision of photogrammetric height measurements; self-calibration was a fortunate by-product. Of the available exposures three were selected from each of the three passes for the purpose of calibration. As illustrated in Figure 1 the selected frames within any one orbit span an arc of approximately 6°, which coupled with the altitude of the spacecraft (108.5km) provided an approximate angle of convergence of 80° between end photographs.

First generation duplicate positive film was provided for the calibration work. Passpoints were marked on all 9 frames with the aid of a Wild PUG 4 by transferring points from the middle frames to the frames at the ends of the arcs. "Dead" areas (i.e. areas not common to all 9 exposures) were marked with supplemental passpoints to obtain a wider distribution of data points over the 55x 55mm format of each frame. In all, there were approximately 170 passpoints. Corners of the imaged format were used as fiducial points for lack of a better reference system.

3.2 Results With Pure Self-calibration

The first reduction performed employed only the photographic measurements as observations. One central exposure was held fixed in an arbitrary position and attitude while all other frames were allowed to adjust relative to this fixed station in the stereotriangulation. Parameters of the inner cone which were also allowed to adjust included c, k_1, p_1, and p_2. Higher order symmetric radial terms were constrained to zero since

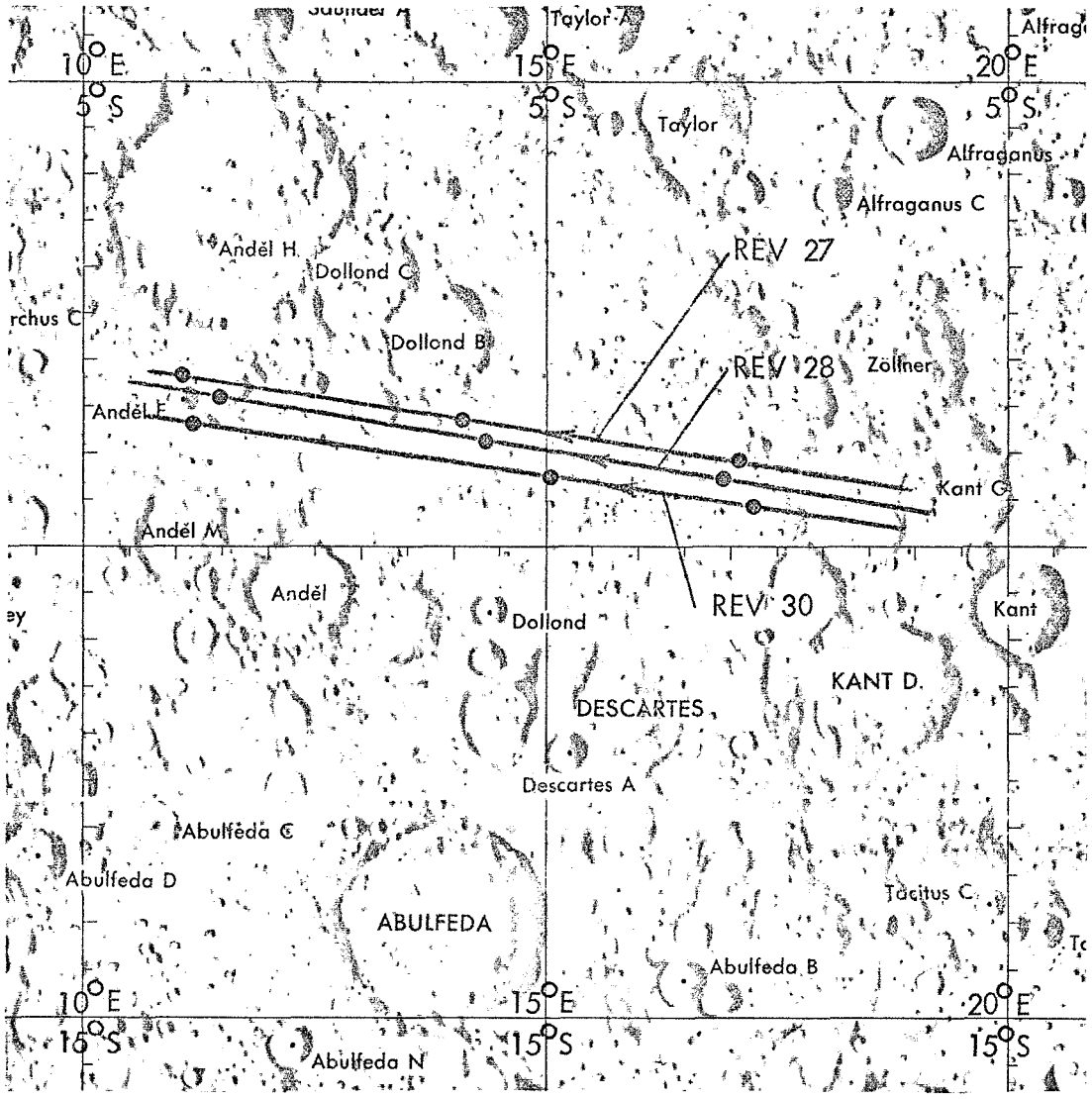

FIGURE 1: Distribution of Photographs Used For In-flight Calibration. Optical axes of end photographs are directed to surface beneath center frames, resulting in an approximate convergence of 80°. Specific frames used are: REV 27-9515, 9525, 9535; REV 28-9556, 9565, 9574; REV 30-9595, 9601, 9615.

a one term Gaussian function completely describes the symmetric radial distortion of the Zeiss Tele-Tessar lens used in the camera. x_p and y_p were also constrained to zero because "incomplete" geometry of the photogrammetric net and the narrow field (8° across diagonals) of the camera would not permit recovery of these parameters (see Section 2.3). The mean error of the photographic measurement residuals for this reduction was 15.8 μm.

Calibration constants derived from the reduction are listed with their posteriori standard deviations in Table 1. Values given for the focal length and symmetric radial distortion terms are "balanced". That is, c' is a calibrated focal length corresponding to the adjusted symmetric radial distortion function now defined by the coefficients k_0' and k_1' in the relation:

$$\delta_r' = k_0' r + k_1' r^3 \qquad (14)$$

where,

δ_r' = balanced symmetric radial distortion in mm; defined to be positive when directed away from the principal point

r = radial distance in mm from the principal point of photogrammetry.

The radial distortion function is balanced such that δ_r' is zero at a radial distance of 30mm, a criterion adopted only to facilitate comparison to a factory calibration of the lens in Section 3.4. The decentering coefficients p_1 and p_2 may be combined to examine the profile (P_r) of maximum tangential distortion by:

$$P_r = (p_1^2 + p_2^2)^{\frac{1}{2}} r^2 . \qquad (15)$$

TABLE 1

Hasselblad Calibration Constants
Derived by Pure Self-calibration

Parameter	Cal. Value	Std. Dev.	Units
c'	502.630	± 2.060	mm
k_0'	$-.14065 * 10^{-1}$	$\pm .58 * 10^{-4}$	-
k_1'	$+.15614 * 10^{-4}$	$\pm .172 * 10^{-6}$	mm^{-2}
p_1	$+.3604 * 10^{-6}$	$\pm .3575 * 10^{-5}$	mm^{-1}
p_2	$+.2998 * 10^{-5}$	$\pm .3020 * 10^{-5}$	mm^{-1}

Evaluations of equations (14) and (15) with calibration data presented in Table 1 are provided in Table 2.

TABLE 2

Evaluation of Balanced Symmetric Radial
and Decentering Distortion by Pure Self-calibration

	Symmetric Radial		Decentering	
r (mm)	δ_r' (μm)	$\sigma\delta_r'$ (μm)	P_r (μm)	σP_r (μm)
0	0	0	0	0
5	- 68	0	0	0
10	-125	1	0	0
15	-158	1	1	1
20	-156	2	2	1
25	-108	3	3	2
30	0	5	4	3
35	+177	8	6	4
39	+378	11	7	5

3.3 Results With External Constraints

During the photographic sequences on each of the three orbits (Figure 1) an attempt was made to precisely record the time of the midpoint of shutter for each exposure. From these timing data the orbital position of the spacecraft at the instant of exposure was to be extracted through a correlation in time with tracking data gathered from earth based stations. As it turned out, the shutter timing data were completely lost for revolution 30, but were acquired successfully for the arcs of revolutions 27 and 28 over Descartes. Positional data derived from earth based tracking were introduced in the self-calibration reduction as parameters subject to a priori constraints.

Since all computations were performed in a rectangular moon-centered coordinate system a covariance matrix to be attached to individual exposure stations was computed according to the technique developed by Gyer (1970). In substance, the approach involves transforming estimated positional standard deviations, expressed in terms of in-track, cross-track and radial components, to a full covariance matrix in the moon-centered system. After several experimental reductions with varying levels of constraints on the exposure stations it was found that the exposures in revolution 27 and 28 could be constrained to 50 and 10 meters, respectively, without contaminating the photogrammetric closures; a mean error of 16.2 μm was achieved.

Parameters of the inner cone derived from this solution are listed in Table 3 and Table 4 represents evaluations of the symmetric radial and decentering profile functions. A comparison of Tables 3 and 4 to Tables 1 and 2 shows quite clearly that exercising constraints on the exposure stations has had virtually no effect upon the recovered calibration. Moreover, only a moderate improvement of the posteriori standard deviations of the parameters of the inner cone has resulted.

TABLE 3

Calibration Constants Derived by
Self-calibration With Positional Constraints

Parameter	Cal. Value	Std. Dev.
c'	504.056	±1.503
k_0'	$-.14144 * 10^{-1}$	$\pm.43 * 10^{-4}$
k_1'	$+.15701 * 10^{-4}$	$\pm.176 * 10^{-6}$
P_1	$+.6542 * 10^{-6}$	$\pm.2454 * 10^{-5}$
P_2	$-.2063 * 10^{-7}$	$\pm.2739 * 10^{-5}$

TABLE 4

Balanced Symmetric Radial and Decentering Distortion
by Self-calibration With Positional Constraints

	Symmetric Radial		Decentering	
r (mm)	δ_r' (μm)	$\sigma\delta_r'$ (μm)	P_r (μm)	σP_r (μm)
0	0	0	0	0
5	- 69	0	0	0
10	-126	0	0	0
15	-159	1	0	1
20	-157	2	0	1
25	-108	3	0	2
30	0	5	1	2
35	+178	8	1	3
39	+380	11	1	4

3.4 Comparison of Calibrations

Prior to shipment to NASA, the 500mm lens was checked for distortion at the Zeiss (Oberkochen) factory. A typical factory-type check was performed by taking measurements at rather widely separated radial distances along the four semi-diagonals of the format. Distortion data reported by Zeiss are given in Table 5. The calibrated focal length corresponding to the data was reported as 507.87 mm with no estimated standard deviation.

TABLE 5

Distortion Data From Factory

	Distortion (μm) for Semi-diagonal				
r(mm)	A	B	C	D	Average
0	0	0	0	0	0
10	-122	-126	-126	-124	-124
20	-145	-153	-152	-149	-150
30	+ 12	- 11	- 2	+ 2	0
39	+404	+375	+381	+393	+388

In addition to the available factory data, NASA has since (after inception of the contract to perform the in-flight calibration) performed a stellar calibration of the camera using the stellar SMAC programs developed by DBA (Brown (1968), Gyer, et. al. (1970)). Calibration coefficients derived from the stellar reduction are shown in Table 6; we have rebalanced NASA's symmetric radial distortion function and calibrated focal

length so that the distortion is zero at a radial distance of 30mm as has been done with the factory as well as our own self-calibration data. Evaluations of the distortion functions from the stellar calibration are given in Table 7.

TABLE 6

Calibration Constants Derived by
Stellar SMAC

Parameter	Cal. Value	Std. Dev.
c'	507.306	±.072
k_0'	$-.14741 * 10^{-1}$	$\pm.2 * 10^{-5}$
k_1'	$+.17241 * 10^{-4}$	$\pm.422 * 10^{-6}$
k_2'*	$-.95765 * 10^{-9}$	$\pm.29277 * 10^{-9}$
p_1	$+.3858 * 10^{-5}$	$\pm.8626 * 10^{-6}$
p_2	$+.1241 * 10^{-5}$	$\pm.8375 * 10^{-6}$

* A two-term Gaussian function was carried in the stellar calibration, leading to a three term balanced function.

TABLE 7

Balanced Symmetric Radial and Decentering Distortion by Stellar SMAC

	Symmetric Radial		Decentering	
r (mm)	δ'_r (μm)	$\sigma\delta'_r$ (μm)	P_r (μm)	σP_r (μm)
0	0	0	0	0
5	- 72	0	0	0
10	-130	0	0	0
15	-164	1	1	0
20	-160	2	2	0
25	-108	4	2	1
30	0	5	4	1
35	+173	5	5	1
39	+361	8	6	1

The radial distortion functions from the three types of calibration are plotted in Figure 2. Although the graph is labeled "symmetric radial distortion" it should be noted that, in the case of the factory calibration, effects of significant decentering distortion are inherent in the average distortion data taken from Table 5. The correspondence of all three curves is extremely close considering that no attempt has been made to match the curves perse; the only normalization applied has been simply to pass all functions through zero at a radial distance of 30mm. As plotted, the SMAC and self-calibration curves lie well with their combined one sigma error bounds except in

FIGURE 2: Comparison of Symmetric Radial Distortion Functions. All curves are balanced such that $\delta'_r = 0$ at 30mm but no additional effort has been made to "match" the curves.

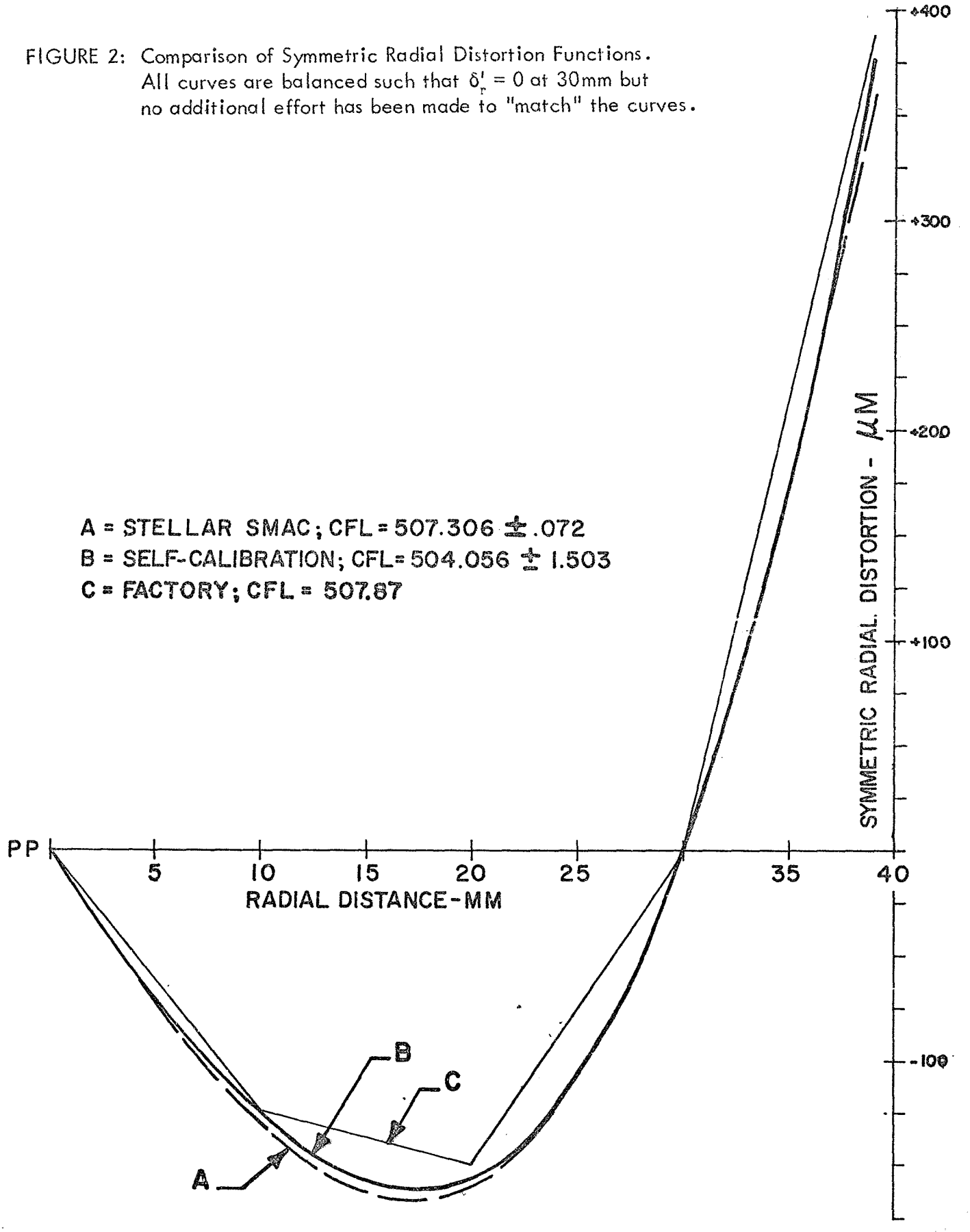

the region between 5 and 20mm radial distance where the difference between the curves is 5 to 6 μm. However, a very slight rebalancing would have the two curves lie completely within their respective one sigma error bounds.

The real item of interest in comparing the two curves lies in the corresponding calibrated focal lengths for it is here that the differences cannot be satisfactorily reconciled on the basis of their respective one sigma standard deviations or by rebalancing. Indeed, a full two sigma adjustment of the focal length from self-calibration is required to bring it into agreement with the value from the SMAC calibration. This result, therefore, necessarily leads to the supposition that the spacecraft rendezvous window, through which the convergent photographs were exposed, has acted as a very weak negative lens element in the photographic system.

With respect to decentering distortion, the profile functions from the two self-calibration reductions (Tables 2 and 4) are not in particulary good agreement although their one sigma error bounds are rather large and do overlap. On the other hand, there is very good agreement between the result from pure self-calibration and that from Stellar SMAC, the maximum discrepancy being only 1 μm (compare Tables 2 and 7). Also of interest is that all three calibrations agree quite well as to the location of the line of maximum tangential distortion within the format of the camera. As derived by Brown (1965) the location of this line is defined by the decentering phase angle φ_0 which is measured positively from the positive x axis toward the positive y axis in the photographic coordinate system. φ_0 is related to p_1 and p_2 by the equation:

$$\varphi_0 = \tan^{-1}\left(\frac{-p_1}{p_2}\right). \qquad (16)$$

Phase angles from the various calibrations are given in Table 8.

TABLE 8

Decentering Phase Angles From Various Calibrations

Calibration	φ_o (deg)	$\sigma\varphi_o$ (deg)
Stellar SMAC	-72	± 12
Pure Self-calibration	-50	± 40
Self-calibration with Position Constraints	-92	±240

4.0 THE POTENTIAL OF IN-ORBIT SELF-CALIBRATION

While the results of the Hasselblad calibration reported in the preceding section are quite admirable, the APOLLO 14 data do not give a complete picture of the power of pure[1] self-calibration because of the narrow cone angle of the camera and the fact that all frames were exposed with the same $\varkappa$ angle. To conclude this paper we wish to demonstrate the full potential of pure self-calibration by presenting results of a series of simulations which have been performed to depict the precision with which a full calibration of the inner cone can be recovered given typical APOLLO orbits, specific exposure configurations, and cone angles.

In the first set of simulations three consecutive low inclination lunar orbits with a spacecraft altitude of 108.5 km are postulated. Three exposures per orbit with 90° increments in $\varkappa$, as illustrated in Figure 3, are assumed; end photographs are exposed during a spacecraft pitch maneuver to provide an 80° angle of convergence. Assuming a photogrammetric error budget of 15 μm and an array of 215 passpoints, simulations have been performed for various

[1] Without external constraints (e.g. orbital).

focal length Hasselblad cameras used on APOLLO missions. Results of these simulations are presented in Table 9 in terms of the posteriori standard deviations of the recovered parameters. In the case of the symmetric radial and decentering profile functions, standard deviations of the functions at the corners of the 55x55mm format have been tabulated for ease of interpretation.

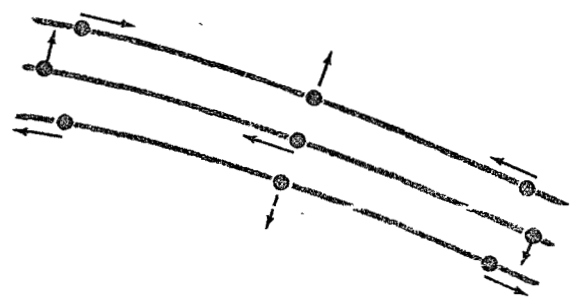

FIGURE 3. Simulated Photographic Sequence For Pure Self-calibration. Orbits are consecutive and of low inclination; spacecraft pitch maneuver allows 80° angle of convergence between end photographs. Arrows indicate camera is rotated 90° between individual exposures.

In analyzing the data presented in Table 9 one should be reminded that an entirely practical situation has been simulated (viz. nine exposures, 80° maximum angle of convergence, 15 μm error budget). Indeed the simulation depicts exactly the circumstances encountered with the APOLLO 14 Hasselblad data, with the lone exception of incremental $\varkappa$ angles. In regard to this requirement it should be mentioned that a special spacecraft maneuver is not required to affect increments of 90° in $\varkappa$. Rather, a simple mounting bracket which will allow a rotation of the camera about its optical axis is all that is required. Moreover, the time interval between successive exposures within one pass is 50 to 60 seconds; ample time to ready the camera between exposures.

TABLE 9

Results of Simulated Self-calibration
For Various Hasselblad Cameras

Focal Length (mm)	Field of View (deg)	Standard Deviation of Recovered Functions				
		x_p (μm)	y_p (μm)	c (μm)	σ_r^* (μm)	$\bar{P}_r^*$ (μm)
50	58×58	9	6	14	15	2
80	38×38	21	14	26	13	2
150	20×20	70	44	70	12	2
500	6× 6	740	460	701	12	2

* At corner of format.

As a final illustration of the power of pure self-calibration a simulation similar to those described above was performed for the metric lunar terrain camera which was successfully flown on the recent APOLLO 15 mission and which is scheduled for the two remaining missions as well. Other than to specify a 3 inch focal length, 4.5x4.5 inch format, and a 5μm error budget, this simulation was geometrically identical to the simulated Hasselblad calibrations. Table 10 summarizes the results, which by their very magnitude require no further elaboration.

TABLE 10

Results of Simulated Self-calibration
For the Lunar Terrain Camera

Parameter	Standard Deviation (μm)
x_p	2
y_p	2
c'	3
δ_r' *	6
P_r *	1

* At corner of format.

REFERENCES

Brown, D.C., 1955. "A Matrix Treatment of the General Problem of Least Squares Considering Correlated Observations", Ballistic Research Labs. Report No. 43.

Brown, D.C., 1958. "A Solution to the General Problem of Multiple Station Analytical Stereotriangulation", RCA Data Reduction Technical Report No. 43, AFMTC-TR-58-8, ASTIA Document No. 134278.

Brown, D.C., Bush, N. and Sibol, J., 1963. "Study of the Feasibility of Satellite Approaches to the Calibration of Tracking Systems", AFCRL Report No. 63-789 prepared by D. Brown Associates, Inc., Melbourne, Florida.

Brown, D.C., Bush, N., and Sibol, J., 1964. "Investigation of the Feasibility of Self-calibration of Tracking Systems", AFCRL Report No. 64-441 prepared by D. Brown Associates, Inc., Melbourne, Florida.

Brown, D.C., Davis, R.G., and Johnson, F.C., 1964. "The Practical and Rigorous Adjustment of Large Photogrammetric Nets", prepared for Rome Air Development Center under Contract AF30(602)-3007, D. Brown Associates, Melbourne, Florida.

Brown, D.C., 1965. "Decentering Distortion of Lenses", paper presented to the Annual Convention of the American Society of Photogrammetry, March 1965. Also published in Photogrammetric Engineering, Vol. XXXII, No. 3.

Brown, D.C., 1968. "Advanced Methods for the Calibration of Metric Cameras", prepared for U.S. Army Engineer Topographic Laboratories under Contract DA-44-009-AMC-1457(X), DBA Systems, Inc., Melbourne, Florida.

Brown, D.C., Kenefick, J.F., and Harp, B.F., 1971. "Photogrammetric Measurements of Explosive Bolts on the Canopy of the OAO Launch Vehicle", prepared for the California Institute of Technology Jet Propulsion Laboratory under Contract HE-527814, Photogrammetric Structural Measurements Report No. 31, DBA Systems, Inc., Melbourne, Florida.

Doyle, F.J., 1970. "Photographic Systems for APOLLO", Photogrammetric Engineering, Vol. XXXVI, No. 10.

Gyer, M.S., 1970. "The Analytical Aerotriangulation of the APOLLO 10 Hasselblad Photography", prepared for NASA Manned Spacecraft Center Mapping Science Laboratory under Contract NAS9-9993, DBA Systems, Inc., Melbourne, Florida.

Gyer, M.S., Haag, N.N., and Llewellyn, S.K., 1970. "Documentation for the Multi-camera Stellar SMAC Computer Program", prepared for U.S. Army Engineer Topographic Laboratories under Contract DAAK02-69-C-0099 by DBA Systems, Inc., Melbourne, Florida.

Kenefick, J.F., 1971. "Ultra Precise Analytical Stereotriangulation for Structural Measurements", paper presented to the Symposium on Close-range Photogrammetry at the University of Illinois, January 1971, DBA Systems, Inc., Melbourne, Florida.